arXiv:1401.2313v1 [math.NA] 10 Jan 2014

A numerical investigation of level sets of extremal Sobolev functions

Stefan Juhnke and Jesse Ratzkin

University of Cape Town

juhnke.stefan@gmail.com and jesse.ratzkin@uct.ac.za

January 13, 2014

Abstract

In this paper we investigate the level sets of extremal Sobolev functions. For $\Omega \subset \mathbf{R}^n$ and $1 \leq p < \frac{2n}{n-2}$, these functions extremize the ratio $\frac{\|\nabla u\|_{L^2(\Omega)}}{\|u\|_{L^p(\Omega)}}$. We conjecture that as p increases the extremal functions become more "peaked" (see the introduction below for a more precise statement), and present some numerical evidence to support this conjecture.

1 Introduction

Let $n \geq 2$, and let $\Omega \subset \mathbf{R}^n$ be a bounded domain with piecewise Lipschitz boundary, satisfying a uniform cone condition. One can associate a large variety of geometric and physical constants to Ω, such as volume, perimeter, diameter, inradius, the principal frequency $\lambda(\Omega)$, and torsional rigidity $P(\Omega)$ (which is also the maximal expected exit time of a standard Brownian particle). For more than a century, many mathematicians have investigated how all these quantities relate to each other; Pólya and Szegő's manuscript [23] provides the best introduction to this topic, which remains very active today, with many open questions.

In the present paper we investigate the quantity

$$\mathcal{C}_p(\Omega) = \inf \left\{ \frac{\int_\Omega |\nabla u|^2 d\mu}{\left(\int_\Omega |u|^p d\mu\right)^{2/p}} : u \in W_0^{1,2}(\Omega), u \not\equiv 0 \right\}. \tag{1}$$

The constant $\mathcal{C}_p(\Omega)$ gives the best constant in the Sobolev embedding:

$$u \in W_0^{1,2}(\Omega) \Rightarrow \|u\|_{L^p(\Omega)} \leq \frac{1}{\sqrt{\mathcal{C}_p(\Omega)}} \|\nabla u\|_{L^2(\Omega)}.$$

By Rellich compactness, the infimum in (1) is finite, positive, and realized by an extremal function u_p^*, which we can take to be positive inside Ω (see, for instance, [12] or [25]). The Euler-Lagrange equation for critical points of the ratio in (1) is

$$\Delta u + \Lambda u^{p-1} = 0, \quad u|_{\partial\Omega} = 0, \tag{2}$$

where Λ is the Lagrange multiplier. In the case that $u = u_p^*$ is an extremal function, a quick integration by parts argument shows that the Lagrange multiplier Λ is given by

$$\Lambda = \mathcal{C}_p(\Omega) \left(\int_\Omega (u_p^*)^p d\mu \right)^{\frac{2-p}{p}}.$$

It is worth remarking that in two cases the PDE (2) becomes linear: that of $p = 1$ and $p = 2$. In the case $p = 1$, we recover the torsional rigidity as $P(\Omega) = (\mathcal{C}_1(\Omega))^{-1}$, and in the case $p = 2$ we recover the principal freqency as $\lambda(\Omega) = \mathcal{C}_2(\Omega)$. These linear problems are both very well-studied, from a variety of perspectives, and the literature attached to each is huge. From this perspective, the second author and Tom Carroll began a research project several years ago, studying the variational problem (1) as it interpolates between torsional rigidity and principal frequency, and beyond. (See, for instance, [4] and [5].) Primarily, we are interested in two central questions:

- Which of the properties of $P(\Omega)$ and $\lambda(\Omega)$ (and their extremal functions) also hold for $\mathcal{C}_p(\Omega)$ (and its extremal functions)?
- Can we track the behavior of $\mathcal{C}_p(\Omega)$ and its extremal function u_p^* as p varies?

Some of our invegistgations have led us conjecture the following.

Conjecture 1. *Let $n \geq 2$ and let $\Omega \subset \mathbf{R}^n$ be a bounded domain with piecewise Lipschitz boundary satisfying a uniform cone condition. Normalize the corresponding (positive) extremal function u_p^* so that*

$$\sup_{x \in \Omega} (u_p^*(x)) = 1,$$

and define the associated distribution function

$$\mu_p(t) = |\{x \in \Omega : u_p^*(x) > t\}|.$$

Then within the allowable range of exponents we have the inequality

$$1 \leq p < q \Rightarrow \mu_p(t) > \mu_q(t) \quad \text{for almost every } t \in (0,1). \tag{3}$$

If $n = 2$ *the allowable range of exponents is* $1 \leq p < q$*,and if* $n \geq 3$ *the allowable range of exponents is* $1 \leq p < q < \frac{2n}{n-2}$.

Below we will present some compelling numerical evidence in support of this conjecture. The remainder of the paper is structured as follows. In Section 2 we provide some context for our present investigation, and describe some of the related work present in the literature. In Section 3 we describe the numerical method we use, as well as its theoretical background, and we present our numerical results in Section 4. We conclude with a brief discussion of future work and unresolved questions in Section 5.

ACKNOWLEDGEMENTS: Most of the work described below comes from the first author's honors dissertation, completed under the direction of the second author. J. R. is partially supported by the National Research Foundation of South Africa.

2 Related results

In this section we will highlight some related theorems about principal frequency, torsional rigidity, qualitative properties of extremal functions, and other quantities. The following is by no means an exhaustive list.

The distribution function μ_p is closely related to a variety of rearrangements of a generic test function u for (1). One can rearrange the function values of a positive function in a variety of ways, and different rearrangements will yield different results. One of the most well-used rearrangements is Schwarz symmetrization, where one replaces a positive function u on Ω with a radially-symmetric, decreasing function u^* on B^*, a ball with the same volume as Ω. The rearrangement is defined to be equimeasurable with u:

$$|\{u > t\}| = |\{u^* > t\}| \text{ for almost every function value } t.$$

Krahn [14] used Schwarz symmetrization to prove an inequality conjectured by Rayleigh in the late 1880's:

$$\lambda(\Omega) \geq \left(\frac{|\Omega|}{\omega_n}\right)^{-2/n} \lambda(\mathbf{B}), \tag{4}$$

where $\mathbf{B}$ is the unit ball in $\mathbf{R}^n$, and ω_n its volume. Moreover, equality can only occur in (4) if $\Omega = \mathbf{B}$ apart from a set of measure zero. In fact, it is straightforward to adapt Krahn's proof to show

$$|\Omega| = |\mathbf{B}| \Rightarrow \mathcal{C}_p(\Omega) \geq \mathcal{C}_p(\mathbf{B}), \tag{5}$$

with equality occuring if and only if $\Omega = \mathbf{B}$ apart from a set of measure zero (see [4]). One can also use similar techniques to prove, for instance, that the square has the greatest torsional rigidity among all rhombi of the same area [22].

However, there is certainly a limit to the results one can prove using only Schwarz (or Steiner) symmetrization, and to go further one must apply new techniques. Among these, one can rearrange by weighted volume [21, 24, 13], which works well for wedge-shaped domains. One can rearrange by powers of u, or (more generally) by some function of the level sets of u [19, 20, 26, 6]. If one is combining domains using Minkowski addition, then the Minkowski sup-convolution is a very useful tool [8].

All these techniques are successful, to varying degrees, when studying (1) for a **fixed** value of p. However, we are presently at a loss with regards to applying them when allowing p to vary. There are comparitively few results comparing the behavior of $\mathcal{C}_p(\Omega)$ and its extremals u_p^* for different values of p.

It is well-known [27] that as $p \to \frac{2n}{n-2}$ the solutions u_p^* become arbitrarly peaked, and the distribution function $\mu_p(t)$ approaches 0 on the interval $(\epsilon, 1)$ for any $\epsilon > 0$. This behavior is a reflection of the fact that the Sobolev embedding is not compact for the critical exponent of $\frac{2n}{n-2}$, and the loss of compactness is due to the fact that the functional in (1) is invariant under conformal transformation for this exponent. Thus, it is interesting to understand the asymptotics as $p \to \frac{2n}{n-2}$. A partial list of such results includes an asymptotic expansion of $\mathcal{C}_p(\Omega)$ due to van den Berg [3] and a theorem of Flucher and Wei [10] (see also [2]) determining the asymptotic location of the maximum of the extremal u_p^*. Additionally, P. L. Lions [16, 17] started a program to understand the loss of compactness, due to concentration of solutions, for a variety of geometric problems in functional analysis and PDE. R. Schoen and Y.-Y. Li (among others) have exploited this concentration-compactness phenomenon to understand the problem of prescribing the scalar curvature of a conformally flat metric.

We remark that until now we had scant evidence for Conjecture 1. Namely, we knew in advance that the extremals become arbitrarily peaked as p approaches the critical exponent, and we knew that in the very special case $\Omega = \mathbf{B}$ we have $\mu_1(t) > \mu_2(t)$.

3 Our numerical algorithm

Our numerical method is borrowed from foundational work of Choi and McKenna [7] and Li and Zhou [15], and its theoretical underpinning is the famous "mountain pass" method of Ambrosetti and Rabinowitz [1]. Within our range of allowable exponents, Rellich compactness exactly implies that the

functional (1) satisfies the Palais-Smale condition, and so the mountain pass theorem of [1] implies the existence of a minimax critical point. A later refinement of Ni [18] implies that in fact a minimax critical point lies on the Nehari manifold, defined by

$$\mathcal{M} = \left\{ u \in W_0^{1,2}(\Omega) : u \not\equiv 0, \int_\Omega |\nabla u|^2 - u^p d\mu = 0 \right\}. \tag{6}$$

To find critical points, we project onto $\mathcal{M}$, using the operator

$$P_{\mathcal{M}}(u) = \left(\frac{\int_\Omega |\nabla u|^2 d\mu}{\int_\Omega |u|^p d\mu} \right)^{\frac{1}{p-2}} u. \tag{7}$$

Our goal will be to find mountain pass critical points of the associated functional

$$\mathcal{I}(u) = \int_\Omega \frac{1}{2}|\nabla u|^2 - \frac{1}{p}|u|^p d\mu, \tag{8}$$

which lie on the Nehari manifold defined in (6). Observe that the Frechet derivative of $\mathcal{I}$ is

$$\begin{aligned} \mathcal{I}'(u)(v) &= \left. \frac{d}{d\epsilon} \right|_{\epsilon=0} \mathcal{I}(u + \epsilon v) \\ &= \int_\Omega \langle \nabla u, \nabla v \rangle - u^{p-1} v d\mu, \end{aligned}$$

so that, after integrating by parts, we can find the direction v of steepest descent by solving the equation

$$2\lambda \Delta v = -\Delta u - u^{p-1}. \tag{9}$$

We are free to choose $\lambda > 0$ as a normalization constant, and choose it so that $\int_\Omega |\nabla v|^2 d\mu = 1$. (It is well-known that by the Poincaré inequality this H^1-norm is equivalent to the $W^{1,2}$-norm.) An expansion of the difference quotient (using our normalization of v) shows

$$\frac{\mathcal{I}(u + \epsilon v) - \mathcal{I}(u)}{\epsilon} = -2\lambda + \mathcal{O}(\epsilon),$$

so choosing $\lambda > 0$ does indeed correspond to the direction of steepest descent of $\mathcal{I}$, rather than the direction of largest increase.

At this point we remark on the importance of taking $p > 2$. In the superlinear case $u_0 \equiv 0$ is a local minimum and, so long as $u \not\equiv 0$ we have $\mathcal{I}(ku) < 0$ for $k > 0$ sufficiently large. Thus, for any path $\gamma(t)$ joining u_0 to ku_{guess}, the function $h_\gamma(t) = \mathcal{I}(\gamma(t))$ will have a maximum at some value t_γ. We can imagine varying the path γ and finding the lowest such maximal value, which is exactly our mountain pass critical point.

We will begin with an initial guess u_{guess} which is positive inside Ω and 0 on $\partial\Omega$, and let $u_1 = P_{\mathcal{M}}(u_{\text{guess}})$. Thereafter we apply the following algorithm:

1. Given u_k, we compute the direction of steepest descent v_k using (9).

2. If $\|v_k\|_{W^{1,2}(\Omega)}$ is suffiently small we stop the algorithm, and otherwise we let $u_{k+1} = P_{\mathcal{M}}(u_k + v_k)$

3. If $\mathcal{I}(u_{k+1}) < \mathcal{I}(u_k)$ then we repeat the entire algorithm starting from the first step. Otherwise we replace v_k with $\frac{1}{2}v_k$ and recompute u_{k+1}.

4. Upon the completion of this algorithm, we test our numerical solution to verify that it does indeed solve the PDE (2) weakly.

Several remarks are in order. The algorithm outlined above is exactly the one proposed by Li and Zhou in [15]. They proved convergence of the algorithm under a wide variety of hypotheses, which include the superlinear ($p > 2$) case of (1) and (8). However, they do not claim convergence of the algorithm in the sublinear case, and in this case the algorithm fails. On the other hand, we are able to verify that in the superlinear case the algorithm coverges to a positive (weak) solution of the PDE (2), so we are confident we have reliable data in this case. We present this data in the next section.

In this algorithm we must repeatedly solve the linear PDE (9), which we do in the weak sense, using biquadratic (nine-noded) quadrilateral finite elements. In each of these steps we replace the corresponding integrals with sums over the corresponding elements. We outline this numerical step in the paragraphs below.

In this computation we take u as known at the mesh points (by an initial guess or by the result of a previous iteration). Writing $\overline{v} = 2\lambda v + u$, the solution to (9) is given by the solution to

$$\Delta \overline{v} = -u^{p-1} \tag{10}$$

from which we can recover the steepest descent direction v.

To solve for $\overline{v} \in W_0^{1,2}(\Omega)$ we will solve the weak form of (10), *i.e.*

$$\int_\Omega \nabla w(x) \cdot \nabla \overline{v}(x) dx = \int_\Omega w(x) u(x)^{p-1} dx \tag{11}$$

for any test function $w \in W_0^{1,2}(\Omega)$. We will now derive the finite element formulation based on the methods presented by Fish and Belytschko [9]. We firstly notice that we can split up our integral as a sum of the integrals over the individual element domains Ω^e:

$$\sum_{e=1}^{n_{el}} \left\{ \int_{\Omega^e} \nabla w^e(x) \nabla \overline{v}^e(x) dx - \int_{\Omega^e} w^e(x) (\overline{v}^e(x))^{p-1} dx \right\} = 0.$$

Now we now write our functions w and $\overline{v}$ in terms of their finite element approximations as:

$$w(x) \approx w^h(x) = \boldsymbol{N}(x)\boldsymbol{w}, \qquad \overline{v}(x) \approx \overline{v}^h(x) = \boldsymbol{N}(x)\boldsymbol{d},$$

where $\boldsymbol{N}$ are quadratic shape functions with value 1 at their corresponding mesh point and value 0 at all other mesh points, while $\boldsymbol{w}$, $\boldsymbol{d}$ are vectors of nodal function values. The gradients of w and $\overline{v}$ can then be written as

$$\nabla w \approx \boldsymbol{B}(x)\boldsymbol{w}, \qquad \nabla \overline{v} \approx \boldsymbol{B}(x)\boldsymbol{d},$$

where $\boldsymbol{B}$ are the gradients of the shape functions. We can rewrite the above expressions for the element level as

$$w^e(x) \approx \boldsymbol{N}^e(x)\boldsymbol{w}^e, \quad \overline{v}^e(x) \approx \boldsymbol{N}^e(x)\boldsymbol{d}^e, \quad \nabla w^e \approx \boldsymbol{B}^e(x)\boldsymbol{w}^e, \quad \nabla \overline{v}^e \approx \boldsymbol{B}^e(x)\boldsymbol{d}^e.$$

Rewriting the integral using these approximations leaves us with

$$\sum_{e=1}^{n_{el}} \left\{ \int_{\Omega^e} \boldsymbol{w}^{e^T} \boldsymbol{B}^{e^T}(x)\boldsymbol{B}^e(x)\boldsymbol{d}^e dx - \int_{\Omega^e} \boldsymbol{w}^{e^T} \boldsymbol{N}^{e^T}(x)(\boldsymbol{N}^e(x)\boldsymbol{d}^e)^{p-1} dx \right\} = 0,$$

since $\boldsymbol{B}^e(x)\boldsymbol{w}^{eT} = \boldsymbol{w}^{e^T}\boldsymbol{B}^{e^T}(x)$ and $\boldsymbol{N}^e(x)\boldsymbol{w}^{eT} = \boldsymbol{w}^{e^T}\boldsymbol{N}^{e^T}(x)$. We notice that we can take the constants $\boldsymbol{w}^{e^T}$ and $\boldsymbol{d}^e$ outside of the integral to give

$$\sum_{e=1}^{n_{el}} \boldsymbol{w}^{e^T} \left\{ \int_{\Omega^e} \boldsymbol{B}^{e^T}(x)\boldsymbol{B}^e(x) dx \boldsymbol{d}^e - \int_{\Omega^e} \boldsymbol{N}^{e^T}(x)(\boldsymbol{N}^e(x)\boldsymbol{d}^e)^{p-1} dx \right\} = 0.$$

Letting

$$\boldsymbol{K}^e = \int_{\Omega^e} \boldsymbol{B}^{e^T}(x)\boldsymbol{B}^e(x) dx \quad \text{and} \quad \boldsymbol{f}^e = \int_{\Omega^e} \boldsymbol{N}^{e^T}(x)(\boldsymbol{N}^e(x)\boldsymbol{d}^e)^{p-1} dx$$

and using the gather matrix to write

$$\boldsymbol{w}^e = \boldsymbol{L}^e\boldsymbol{w}, \quad \boldsymbol{d}^e = \boldsymbol{L}^e\boldsymbol{d},$$

we get

$$\boldsymbol{w}^T \left(\sum_{e=1}^{n_{el}} \boldsymbol{L}^{e^T} \boldsymbol{K}^e \boldsymbol{L}^e \boldsymbol{d} - \sum_{e=1}^{n_{el}} \boldsymbol{L}^{e^T} \boldsymbol{f}^e \right) = 0.$$

Further letting

$$K = \sum_{e=1}^{n_{el}} \boldsymbol{L}^{e^T} \boldsymbol{K}^e \boldsymbol{L}^e \boldsymbol{d} \quad \text{and } \boldsymbol{f} = \sum_{e=1}^{n_{el}} \boldsymbol{L}^{e^T} \boldsymbol{f}^e = 0,$$

we end up with

$$\boldsymbol{w}^T(\boldsymbol{K}\boldsymbol{d} - \boldsymbol{f}) = 0 \quad \forall \boldsymbol{w}.$$

Since we know that $w \in W_0^{1,2}$ is arbitrary we therefore solve the discrete finite element form

$$\boldsymbol{K}\boldsymbol{d} = \boldsymbol{f}, \tag{12}$$

with $\boldsymbol{N}\boldsymbol{d}$ the finite element approximation to $\overline{v}$ from which we can recover the steepest descent direction v.

4 Numerical results

In this section we describe our numerical results. We implemented the algorithm described in Section 3 using in MATLAB, and all the figures displayed below come from this implementation.

We first implemented our method on a unit ball of dimension four. In this case, the solution is radially symmetric, so we only need to solve an ODE. We display a plot of these solutions in Figure 1.

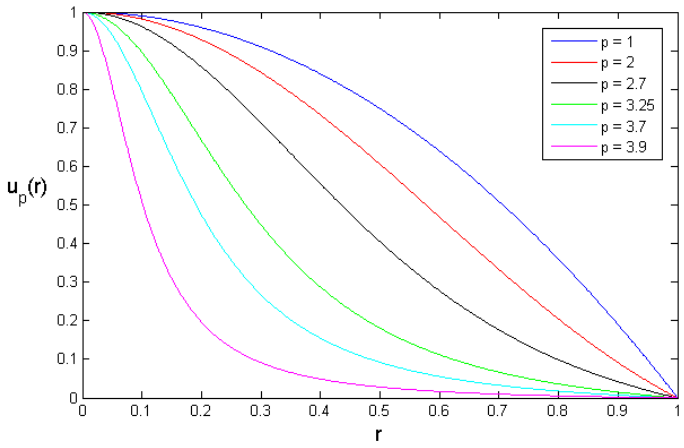

Figure 1: Extremal Sobolev functions for a four-dimensional unit ball

We also display a plot of the corresponding distribution functions in Figure 2.

Observe that, as we expected, the distribution function appears to be monotone, and that as $p \to 4 = \frac{2n}{n-2}$ the solution becomes arbitrarily concentrated at the origin.

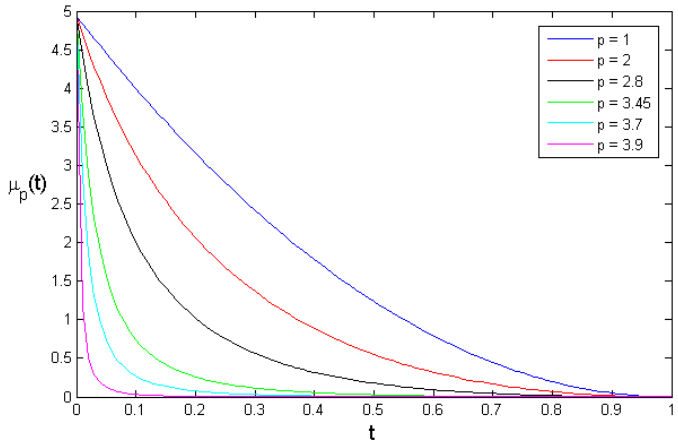

Figure 2: Distributions of extremal Sobolev functions for a four-dimensional unit ball

We can verify that we are indeed finding solutions to the correct PDE. For the case $p = 1$ and $p = 2$ we can compute the solutions analytically, and verify directly that our numerical solution agrees quite well. These are (up to a constant multiple)

$$u_1^*(r) = 1 - r^2, \qquad u_2^*(r) = r^{\frac{2-n}{2}} J_{\frac{n-2}{2}} \left(j_{\frac{n-2}{2}} r \right),$$

where J_a is the Bessel function of the first kind of index a and j_a is its first positive zero. For other values of p we can verify that we have found a weak solution of (2). As the solution is *a priori* radial, we know that the weak form of the PDE is

$$WT_w(u) := \int_0^1 \left[- r^{1-n} \frac{\partial w(r)}{\partial r} \left(r^{n-1} \frac{\partial u(r)}{\partial r} \right) + w(r) \Lambda u(r)^{p-1} \right] r^{n-1} dr = 0 \tag{13}$$

The above lends itself well to testing via finite element approximation. A random test function $w(r)$ is created by randomly generating numbers at the mesh points and $WT_w(u)$ is evaluated by Gauss quadrature. For comparison purposes, the functions u are normalized so that $\sup(u) = 1$. This requires that Λ be rescaled (Λ is set equal to 1 in the algorithm for simplicity), and the appropriate rescaling is then given by a^{2-p} where a is the factor normalizing u. This rescaling is derived from the fact that if u solves

$$\Delta u + u^{p-1} = 0 \tag{14}$$

then au solves

$$\Delta(au) + a^{2-p}(au)^{p-1} = 0,$$

by simply multiplying (14) by a.

We generate values of $WT_w(u)$ for a number of test functions w and examine the average magnitude. As alluded to previously, the result of the test (13) is that for solution candidate functions derived from our algorithm for $2 \leq p < \frac{2n}{n-2}$ and for $p = 1$, we have $WT_w(u)$ very close to zero, meaning that we can be confident that we have found appropriate solutions.

Next we implemented our algorithm in a unit square in the plane. We plot below our numerical solution for both $p = 4$ (Figure 3) and $p = 8$ (Figure 4), and the distribution function for several values of p (Figure 5).

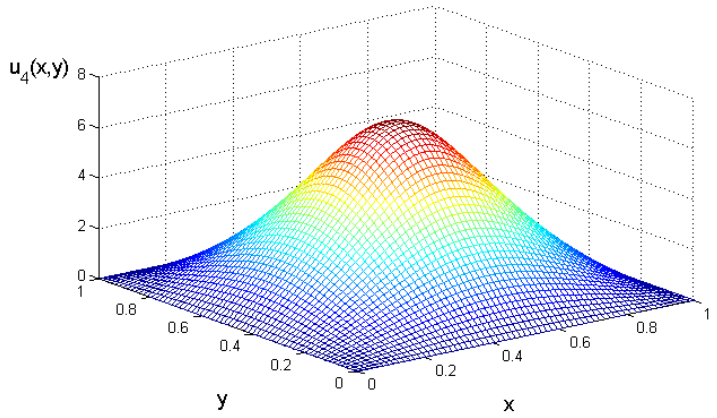

Figure 3: Extremal Sobolev function for $p = 4$ on a unit square

Again we verify that our numerical algorithm does find a weak solution of (2). This time we define

$$WT_w(u) := \int_\Omega [-\nabla u(x)\nabla w(x) + w\Lambda u(x)^{p-1}]dx \tag{15}$$

and again compute $WT_w(u)$ for our candidate solutions, with appropriate rescalings as described previously. We have closely matched the result of Choi and McKenna for the case $p = 4$, which means that we should be able to use the value $WT_w(u_4^*)$ as a gauge for how close to zero $WT_w(u)$ should be for appropriate solutions. Again we find that for $2 \leq p < \frac{2n}{2-n}$ and $p = 1$ we get values of $WT_w(u)$ very close to zero and of the same magnitude as $WT_w(u_4^*)$.

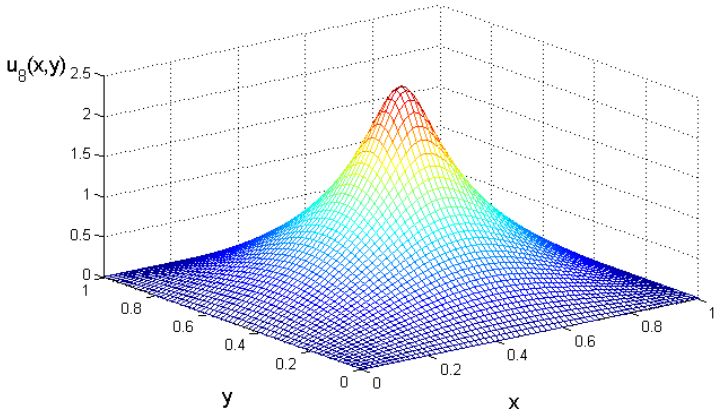

Figure 4: Extremal Sobolev function for $p = 8$ on a unit square

Finally we implemented our algorithm on a rectangle of width 1 and length 4 in the plane. Below we plot the our numerical solutions for $p = 2$ (Figure 6), $p = 4$ (Figure 7), and $p = 8$ (Figure 8), as well as the distribution function for several values of p (Figure 9). We use the same test as we did in the case of the unit square to verify that in the case of he 1×4 rectangle we have indeed found (weak) numerical solutions of (2).

5 Outlook

The present paper is only the start of our numerical and theoretical investigations into Conjecture 1. We would like to verify our results on some more planar domains, such as triangles and parallelograms. Next we anticipate numerical compuations for higher dimensional objects, such as cubes and parallelpipeds, in the super-linear case, as well as possibly some ring domains. We will also need to develope a new numerical algorithm which yields reliable results for $1 < p < 2$. Finally, we hope that our numerical data provides enough insight to rigorously prove our conjecture.

References

[1] L. Ambrostetti and P. Rabinowitz. *Dual variational methods in critical point theory and applications.* J. Funct. Anal. **14** (1973), 349–381.

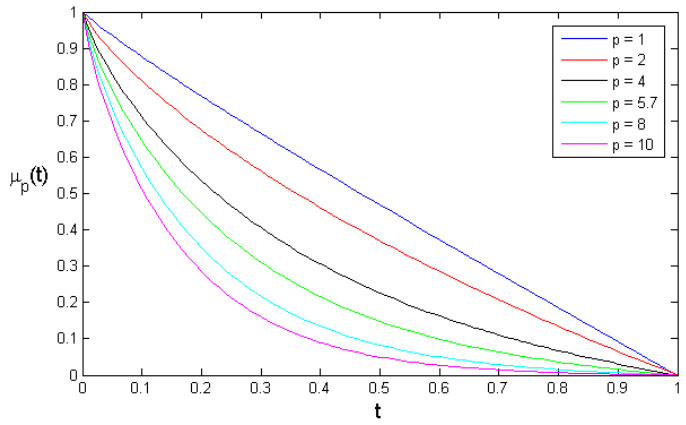

Figure 5: Distributions of extremal Sobolev functions for a unit square in the plane

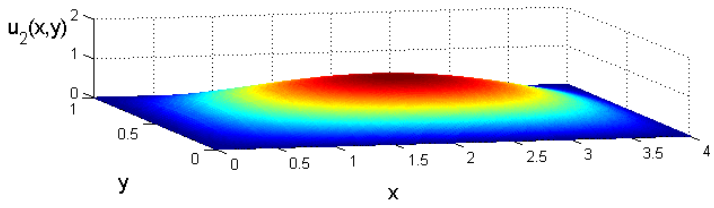

Figure 6: Extremal Sobolev function for $p = 2$ on a 1×4 rectangle

[2] C. Bandle and M. Flucher. *Harmonic radius and concentration of energy; hyperbolic radius and Liouville's equations* $\Delta U = e^U$ *and* $\Delta U = U^{\frac{n+2}{n-2}}$. SIAM Rev. **38** (1996), 191–238.

[3] M. van den Berg. *Estimates for the torsion function and Sobolev constants.* Potential Anal. **36** (2012), 607–616.

[4] T. Carroll and J. Ratzkin. *Interpolating between torsional frequency and principal frequency.* J. Math. Anal. Appl. **379** (2011), 818–826.

[5] T. Carroll and J. Ratzkin. *Two isoperimetric inequalities for the Sobolev constant.* Z. Angew. Math. Phys. **63** (2012), 855–863.

[6] G. Chiti. *A reverse Hölder inequality for eigenfunctions of linear second order elliptic operators.* Z. Angew. Math. Phys. **33** (1982), 143–148.

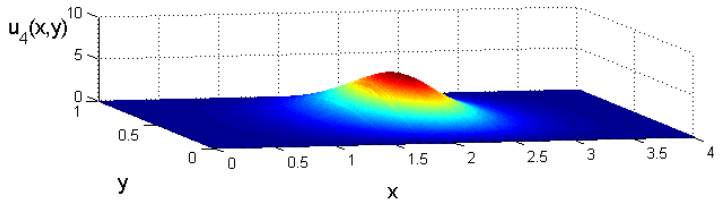

Figure 7: Extremal Sobolev function for $p = 4$ on a 1×4 rectangle

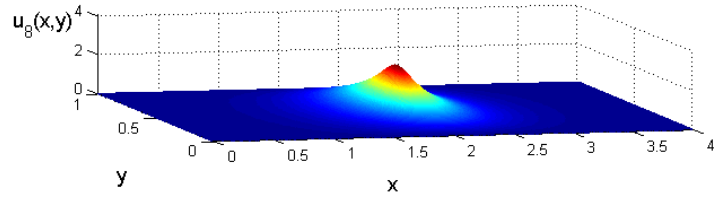

Figure 8: Extremal Sobolev function for $p = 8$ on a 1×4 rectangle

[7] Y. S. Choi and P. J. McKenna. *A mountain pass method for numerical solutions of semilinear elliptic problems.* Nonlinear Anal. **20** (1993), 417–437.

[8] A. Colesanti, P. Cuoghi, and P. Salani. *Brunn-Minkowski inequalities for two functionals involving the p-Laplace operator.* Appl. Anal. **85** (2006), 45–66.

[9] J. Fish and T. Belytschko. *A First Course in Finite Elements.* Wiley (2007).

[10] M. Flucher and J. Wei. *Semilinear Dirichlet problem with nearly critical exponent, asymptotic location of hot spots.* Manuscripta Math. **94** (1997) 337–346.

[11] M. Flucher and J. Wei. *Asymptotic shape and location of small cores in elliptic free-boundary value problems.* Math. Z. **228** (1998), 683–703.

[12] D. Gilbarg and N. Trudinger. *Elliptic Partial Differential Equations of Second Order, Third Edition.* Springer-Verlag (2001).

[13] A. Hasnaoui and L. Hermi. *Isoperimetric inequalities for a wedge-like membrane.* to appear in Ann. Henri Poincaré.

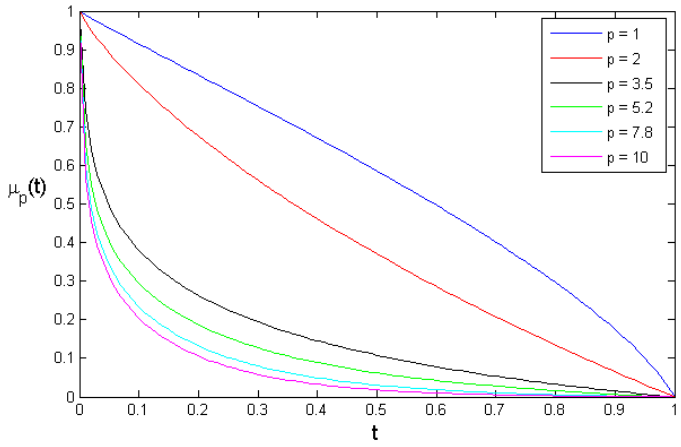

Figure 9: Distributions of extremal Sobolev functions for a 1×4 rectangle

[14] E. Krahn. *Über eine von Rayleigh formulierte Minmaleigenschaft des Kreises.* Math. Ann. **94** (1925), 97–100.

[15] Y. Li and J. Zhou. *A minimax method for finding multiple critical points and its application to semilinear PDEs.* SIAM J. Scientific Computing. **23** (2001), 840–865.

[16] P. L. Lions. *The concentration-compactness principle in the calculus of variations: the locally compact case, part 1.* Ann. Inst. Henri Poincaré **1** (1984), 109–145.

[17] P. L. Lions *The concentration-compactness principle in the calculus of variations: the locally compact case, part2.* Ann. Inst. Henri Poincaré **1** (1984), 223–283.

[18] W.-M. Ni. *Recent progress in semilinear elliptic equations.* RIMS Kôkyûroku Bessatsu **679** (1989), 1–39.

[19] L. Payne and M. Rayner. *An isoperimetric inequality for the first eigenfunction in a fixed membrane.* Z. Angew. Math. Phys. **23** (1972), 13–15.

[20] L. Payne and M. Rayner. *Some isoperimetric norm bounds for solutions of the Helmhotz equation.* Z. Angew. Math. Phys. **24** (1973), 105–110.

[21] L. Payne & H. Weinberger. *A Faber-Krahn inequality for wedge-like membranes.* J. Math. and Phys. **39** (1960) 182–188.

[22] G. Pólya, *Torsional rigidity, principal frequency, electrostatic capacity and symmetrization.* Quarterly J. Applied Math., **6** (1948), 267–277.

[23] G. Pólya and G. Szegő. *Isoperimetric Inequalities in Mathematical Physics.* Princeton University Press (1951).

[24] J. Ratzkin. *Eigenvalues of Euclidean wedge domains in higher dimensions.* Calc. Var. & PDE. **42** (2011), 93–106.

[25] F. Sauvigny. *Partial Differential Equations 1 & 2.* Springer-Verlag, 2003.

[26] G. Talenti. *Elliptic equations and rearrangements.* Ann. Scuola Norm. Sup. Pisa Cl. Sci. (4) **3** (1976), 697–718.

[27] N. Trudinger. *Remarks concerning the conformal deformation of Riemannian structures on compact manifolds.* Ann. Scuola Norm. Sup. Pisa Cl. Sci. (3) **22** 265–274.